Heliyon 9 (2023) e16147

Contents lists available at ScienceDirect

Heliyon

journal homepage: www.cell.com/heliyon

Research article

Integrated analysis of ovarian cancer patients from prospective transcription factor activity reveals subtypes of prognostic significance

Dongqing Su [a], Yuqiang Xiong [a], Haodong Wei [a], Shiyuan Wang [a], Jiawei Ke [a], Pengfei Liang [b], Haoxin Zhang [c], Yao Yu [a], Yongchun Zuo [b,d,**], Lei Yang [a,*]

[a] College of Bioinformatics Science and Technology, Harbin Medical University, Harbin, 150081, China
[b] The State Key Laboratory of Reproductive Regulation and Breeding of Grassland Livestock, College of Life Sciences, Inner Mongolia University, Hohhot, 010070, China
[c] Department of Gastrointestinal Oncology, Harbin Medical University Cancer Hospital, Harbin 150081, China
[d] Digital College, Inner Mongolia Intelligent Union Big Data Academy, Inner Mongolia Wesure Date Technology Co., Ltd., Hohhot, 010010, China

ARTICLE INFO

Keywords:
Ovarian cancer
Immune-related transcription factors
Clustering subtype
Prognosis

ABSTRACT

Transcription factors are protein molecules that act as regulators of gene expression. Aberrant protein activity of transcription factors can have a significant impact on tumor progression and metastasis in tumor patients. In this study, 868 immune-related transcription factors were identified from the transcription factor activity profile of 1823 ovarian cancer patients. The prognosis-related transcription factors were identified through univariate Cox analysis and random survival tree analysis, and two distinct clustering subtypes were subsequently derived based on these transcription factors. We assessed the clinical significance and genomics landscape of the two clustering subtypes and found statistically significant differences in prognosis, response to immunotherapy, and chemotherapy among ovarian cancer patients with different subtypes. Multi-scale Embedded Gene Co-expression Network Analysis was used to identify differential gene modules between the two clustering subtypes, which allowed us to conduct further analysis of biological pathways that exhibited significant differences between them. Finally, a ceRNA network was constructed to analyze lncRNA-miRNA-mRNA regulatory pairs with differential expression levels between two clustering subtypes. We expected that our study may provide some useful references for stratifying and treating patients with ovarian cancer.

1. Introduction

Ovarian cancer is a prevalent gynecological malignancy with the highest mortality rate among all types of genital cancers, causing almost 150,000 female deaths annually [1–4]. The early stages of ovarian cancer do not show any specific symptoms or signs, leading to a vast majority of patients being diagnosed at an advanced stage with metastasis, which, in turn, results in a low 5-year overall survival rate [5–8]. With advancements in next-generation sequencing and molecular biological techniques, ovarian cancer treatment

* Corresponding author. College of Bioinformatics Science and Technology, Harbin Medical University, Harbin, 150081, China.
** Corresponding author. The State Key Laboratory of Reproductive Regulation and Breeding of Grassland Livestock, College of Life Sciences, Inner Mongolia University, Hohhot, 010070, China.
E-mail addresses: yczuo@imu.edu.cn (Y. Zuo), leiyang@hrbmu.edu.cn (L. Yang).

https://doi.org/10.1016/j.heliyon.2023.e16147
Received 17 February 2023; Received in revised form 4 May 2023; Accepted 7 May 2023
Available online 11 May 2023

has entered an era of targeted therapy. Targeted drugs that aim at specific molecular alterations in ovarian cancer have become crucial in maintenance therapy. The conventional therapeutic scheme for ovarian cancer has gradually evolved towards comprehensive chemotherapy, typically involving cytoreductive surgery plus platinum-based drugs and supplemented by molecularly targeted inhibitors [9–12]. Although the current complete remission rate of ovarian cancer is as high as 60–80%, nearly 50% of patients develop chemoresistance or experience recurrence at a later stage [13]. Thus, studies are needed to explore new prognostic markers for ovarian cancer, stratify patients based on biomarkers, and develop new treatment strategies.

Transcription factors are DNA-binding proteins on specific nucleotide sequences upstream of genes [14–18]. They not only bind to non-coding DNA elements to activate or inhibit gene expression but also promote the transcription of mRNAs and functional non-coding RNAs [19,20]. Recent studies have demonstrated that transcription factors are implicated in a broad spectrum of human diseases and can act as oncogenes, exerting critical functions in the pathogenesis of various types of cancer [21]. Furthermore, transcription factors can promote tumor growth and metastasis by participating in diverse important signaling pathways [22–26]. Clinical studies have demonstrated that molecular inhibitors that directly or indirectly inhibit transcription factors can effectively treat various types of cancer. Thus, transcription factors are valuable biomarkers and therapeutic targets. To develop new therapeutic options for patients with cancer, it is crucial to identify aberrantly regulated transcription factors that promote tumorigenesis.

Transcription factor activity is a critical determinant of gene transcriptional regulation. Abnormal activity levels of transcription factors can alter the transcription rate and affect the expression of their target genes [27]. Therefore, the activities of transcription factors have been widely evaluated in recent years. Based on changes in the target gene expression levels of transcription factors, algorithms and analysis tools have been developed for evaluating transcription factor activity [28–31]. However, the activity levels of transcription factors in ovarian cancer are not well-understood, and neither are their prognostic nor therapeutic effects on ovarian cancer [7,8,32,33]. In this study, we constructed transcription factor activity profiles of ovarian cancer using the VIPER algorithm. Following this, distinct subtypes of transcription factor activity were identified to investigate variations in overall survival, genomic characteristics, and therapeutic responses across these subtypes. Encouraging outcomes were observed across different ovarian cancer subtypes, and these findings have the potential to inform clinical treatment guidelines and facilitate personalized approaches for treating patients with ovarian cancer. The workflow of our study was illustrated in Fig. S1.

2. Material and method

2.1. Publicly available datasets

In this study, the gene expression profiles and clinical information of ovarian cancer samples were obtained from multiple sources, including Gene Expression Omnibus (GEO), The Cancer Genome Atlas (TCGA), ArrayExpress database, curatedOvarianData, and published literature in PubMed. After excluding ovarian cancer cohorts with less than 40 samples and those without available overall survival information, a total of 2308 ovarian cancer samples from 15 cohorts were included in our study. Detailed information regarding the processing of these ovarian cancer cohorts was provided in our previous work [34]. Each cohort utilized in this study was processed and analyzed independently. The TCGA, GSE13876, GSE17260, GSE26193, GSE26712, GSE49997, GSE9891, GSE51088, GSE32062, and EMTAB386 [35] cohorts were used as the training cohort. Five ovarian cancer cohorts, including GSE14764, GSE18520, GSE30161, GSE32063, and OVAU [9] cohorts were obtained from distinct platforms to establish the testing cohort for verifying the transcription factor subtypes. The read count data of TCGA ovarian cancer samples were also obtained from the cBioPortal database [36] for the purpose of conducting the differential expression analysis.

2.2. The transcription factor activity profile

The 1332 human transcription factors and their corresponding targets were obtained from the R package dorothea (version 1.6.0) [37]. The human transcription factors and their transcriptional targets of this package were curated and collected from different types of evidence. The VIPER algorithm from the dorothea R package (version 1.6.0) was utilized to calculate the transcription factor activities using the dorothea regulons [38]. The normalized enrichment scores (NESs) were used to represent the levels of human transcription factor activities in the ovarian cancer samples. The positive NES indicated a higher relative protein activity in the ovarian cancer samples, whereas the negative NES indicated a lower relative protein activity in the ovarian cancer samples. Each ovarian cancer cohort was analyzed independently. The NESs of different ovarian cancer cohorts within the training and testing cohorts were merged separately. To ensure the accuracy of the analysis, the ComBat function of the R package sva (version 3.46.0) was utilized to eliminate any possible batch effects that might exist among the NESs of different cohorts within the training and testing cohorts.

2.3. Differentially expressed gene analysis and gene set enrichment analysis

The R package edgeR (version 3.34.1) was utilized to identify the differentially expressed genes between two clustering subtypes in the TCGA cohort [39–41]. The Gene Ontology (GO) and KEGG pathway enrichment analysis were performed on these differentially expressed genes by R package clusterProfile (version 4.4.4) [42]. After setting the criteria of P-value<0.05 and $|\log_2 FC|>1.0$, the GO biological process enriched terms and KEGG enriched pathways were visualized by R package ggplot2 (version 3.3.5).

Using the expression profiles, the relative infiltration of 17 ImmPort immune cell signatures was calculated by the single sample gene set enrichment analysis (ssGSEA) [43] in the ovarian cancer training cohort. Gene set enrichment analysis (GSEA) [44] was conducted to evaluate the enrichment of gene signatures using the GSEA function in R package clusterProfile (version 4.4.4) [42]. 50

Hallmark gene signatures (version 7.5.1) [45] and 17 ImmPort immune cell signatures [46] were chosen as the reference gene sets of GSEA.

2.4. Bioinformatics analysis

Co-expression networks of the ovarian cancer training cohort were constructed using the R package WGCNA (version 1.71) [47]. An appropriate soft threshold power beta value was selected to meet the criteria for the scale-free network. Furthermore, the adjacency matrix was transformed into a topological overlap matrix (TOM). Then, according to the dissimilarity measure derived from TOM, transcription factors were classified into distinct modules.

In order to identify distinct modules in WGCNA, the minimal module size was defined as 30 and the cut height was defined as 0.25.

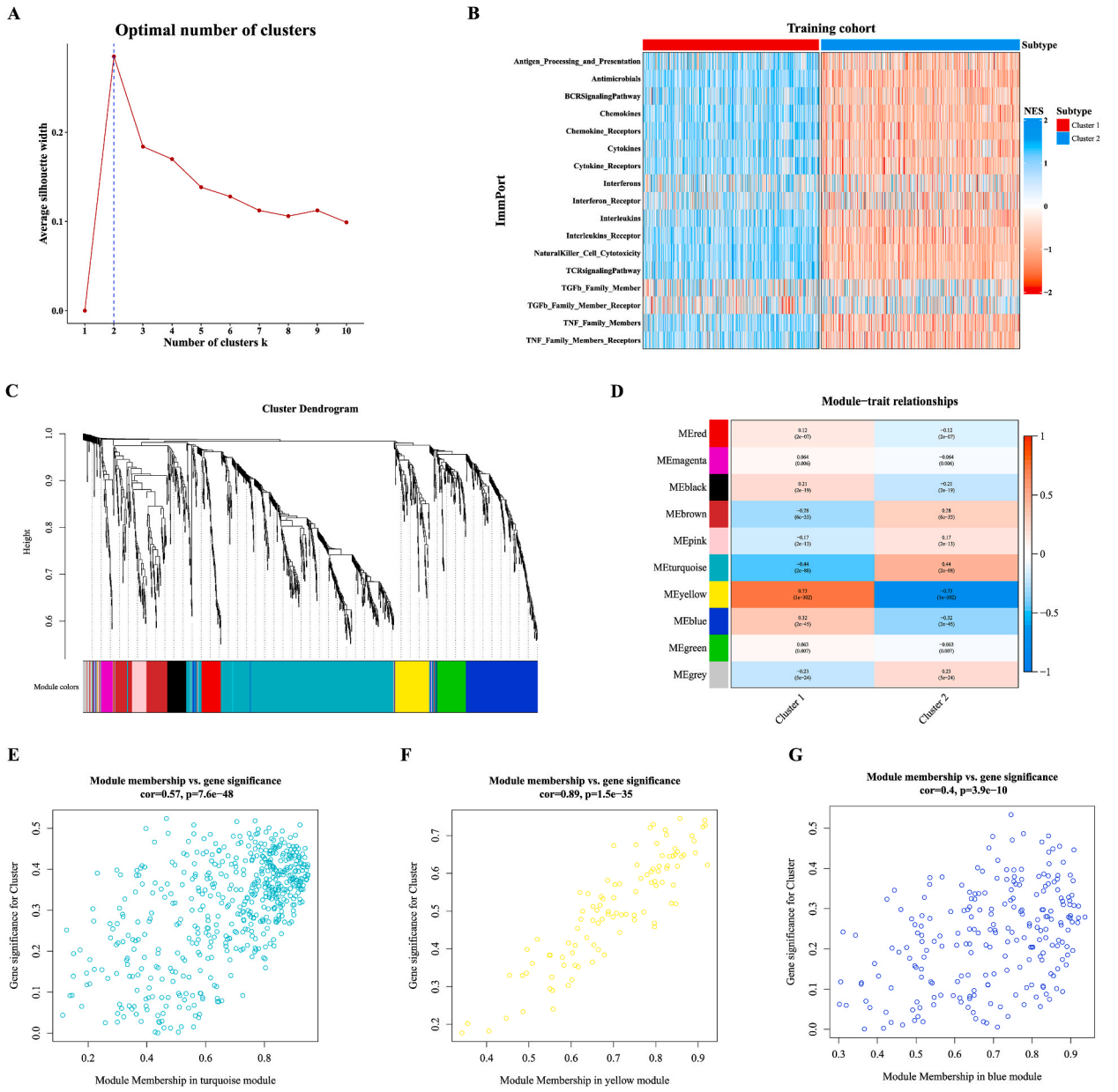

Fig. 1. Identification of immune-related transcription factors in the training cohort. **(A)** The average silhouette width of K-means clustering was calculated for each value of k. The optimal number of clusters was identified as k = 2. **(B)** The infiltration levels of 17 immune cells for the two identified clusters. **(C)** The clustering dendrogram and module division of transcription factors in WGCNA. **(D)** The module-trait relationships between transcription factor modules and two immune clustering subtypes in WGCNA. The correlations between gene significance and module membership in the **(E)** turquoise, **(F)** yellow, and **(G)** blue modules.

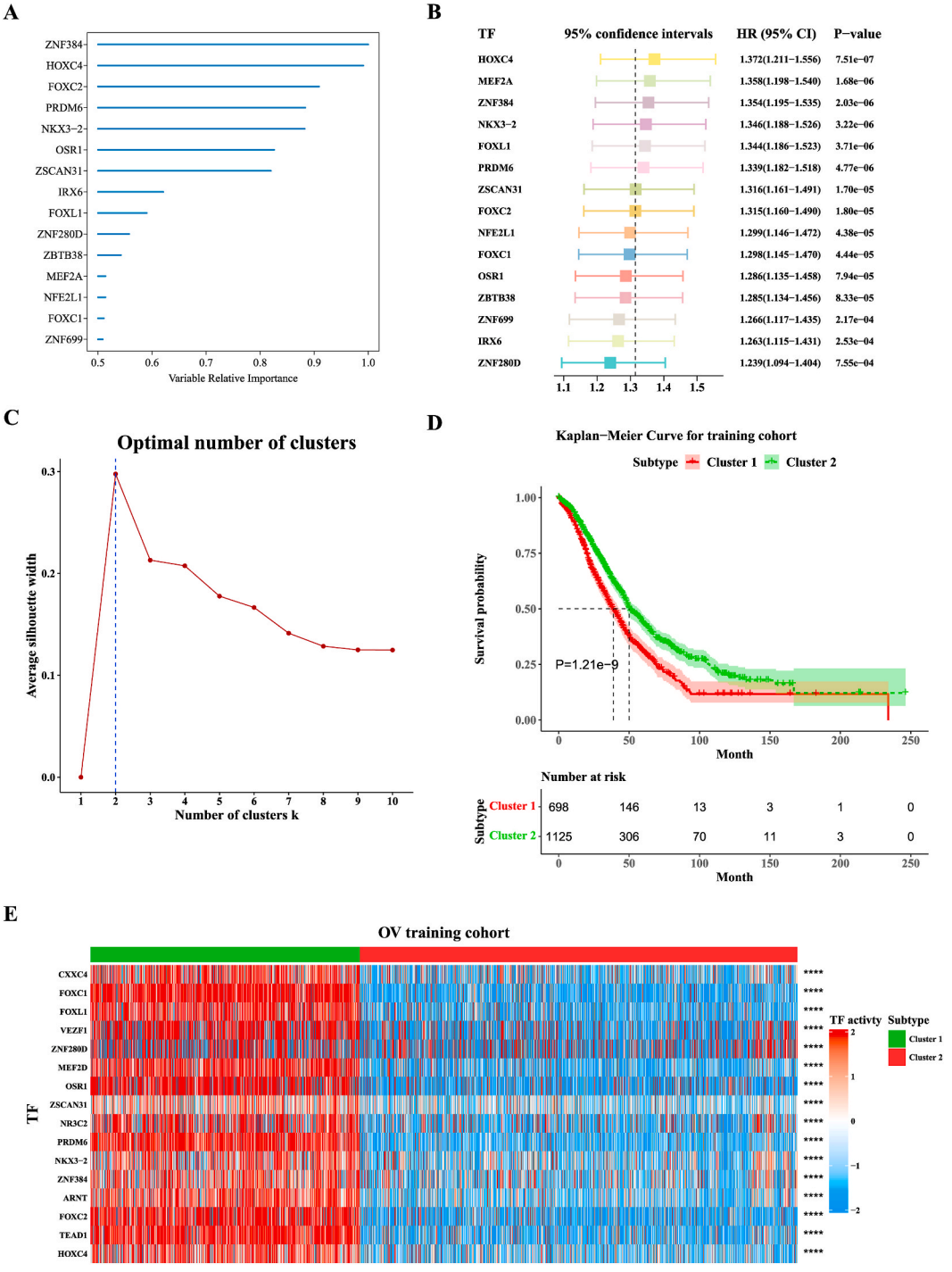

Fig. 2. Construction of two transcription factor activity subtypes in the training cohort. **(A)** The variable relative importance for 15 top-rank transcription factors in random survival tree analysis. **(B)** Forestplot illustrated the 95% confidence intervals, hazard ratio (HR), and *P*-value of 15 transcription factors in the univariate Cox regression analysis. **(C)** The average silhouette width of K-means clustering for each k. The optimal number of the cluster was identified when k = 2. **(D)** Kaplan-Meier curves for two clustering subtypes in the training cohort. **(E)** Heatmap illustrated the protein activity of 15 transcription factors for two clustering subtypes in the training cohort. In this figure, TF indicated transcription factor, OV indicated ovarian cancer, and *** indicated *P*-value<0.001 (Wilcoxon rank-sum test).

The transcription factor modules with the highest correlation with two immune-related clusters were identified as the key modules and were subsequently chosen for further investigation. Then, univariate Cox regression analysis was used in screening variables from the transcription factor activity profile to select prognostic-related transcription factors in the ovarian cancer training cohort. The random survival tree analysis with 1000 trees was trained through the R package randomForestSRC (version 3.1.1) to rank the important variables by the function rfsrc. The K-means clustering was utilized to discover distinct clusters within the ovarian cancer training cohort. The cluster numbers was ranged from 2 to 10, and the silhouette width was adopted as an evaluation metric to determine the optimal number of clusters during the clustering process. The chemotherapeutic sensitivity of eight commonly used anticancer drugs in the Genomics of Drug Sensitivity in Cancer (GDSC) database [48] for the TCGA ovarian cancer samples was obtained from the study of Jia et al. [49]. The Tumor Immune Dysfunction and Exclusion (TIDE) website (http://tide.dfci.harvard.edu/) was utilized to predict the clinical response of immune checkpoint blockade therapy in ovarian cancer samples [50].

2.5. Statistical analysis and software

In this study, the Log-rank test was utilized to evaluate statistical differences in overall survival between two subtypes of ovarian cancer. Furthermore, the R package survminer (version 0.4.9) was utilized to generate visually appealing Kaplan-Meier survival curves. The Wilcoxon rank-sum test was conducted for comparison of variables between the two ovarian cancer subtypes. All statistical analyses were conducted using R software (version 4.0.2) or Python package (version 3.9). All tests were two-tailed, and *P*-values less than 0.05 were considered statistically significant.

3. Results

3.1. Identification of transcription factor modules derived from immunophenotypes

In the ovarian cancer training cohort, the K-means clustering was performed on the infiltration levels of 17 immune cells to identify robust classifications. To determine the optimal number of clusters, the silhouette width curve plot was evaluated for different values of k, ranging from 2 to 10 (Fig. 1A). Fig. 1A illustrated that the optimal number of clusters was achieved when k = 2. So, two ovarian

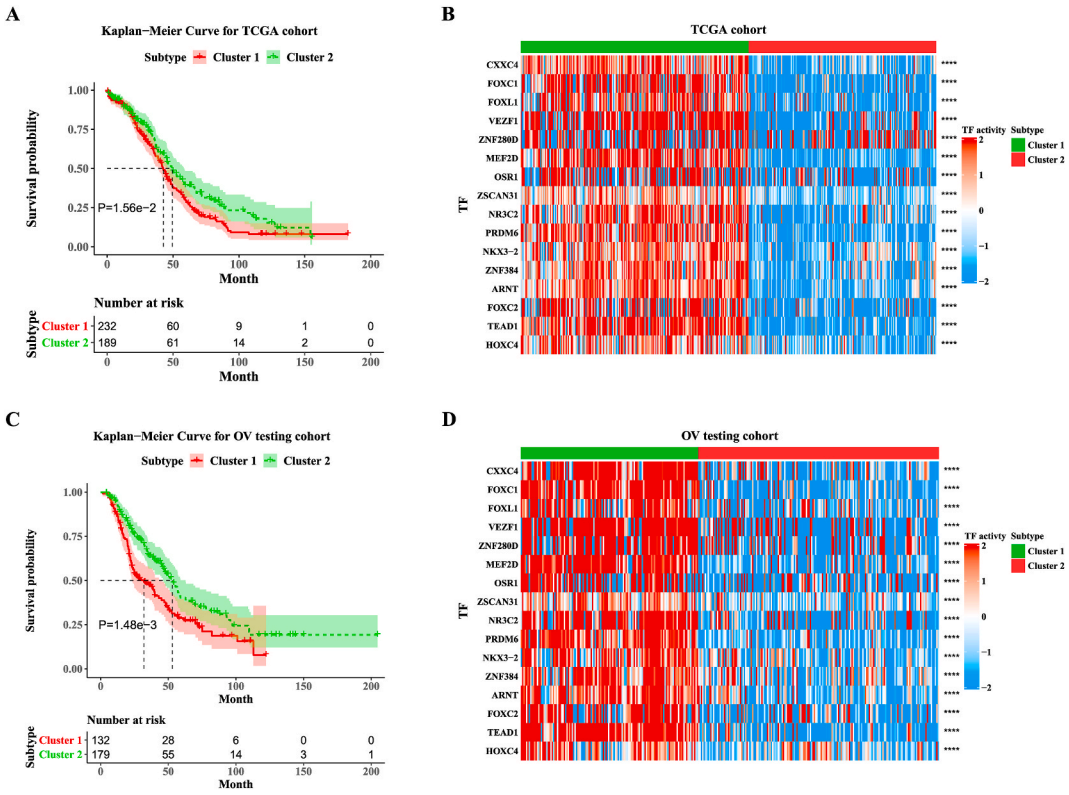

Fig. 3. Validation of the clustering subtypes in the TCGA cohort and testing cohort. **(A)** Kaplan-Meier curves for two clustering subtypes in the TCGA cohort. **(B)** Heatmap illustrated the protein activity of 15 transcription factors for two clustering subtypes in the TCGA cohort. **(C)** Kaplan-Meier curves for two clustering subtypes in the testing cohort. **(D)** Heatmap illustrated the protein activity of 15 transcription factors for two clustering subtypes in the testing cohort. In this figure, TF indicated transcription factor, OV indicated ovarian cancer, and *** indicated *P*-value<0.001 (Wilcoxon rank-sum test).

cancer clusters with distinct immunophenotypes were identified. As illustrated in Fig. 1B, patients with ovarian cancer in cluster 1 exhibited an immune-hot phenotype, characterized by higher levels of immune infiltrates. Conversely, patients with ovarian cancer in cluster 2 demonstrated an immune-cold phenotype, as evidenced by low levels of immune infiltrates (Fig. 1B).

In order to identify the key transcription factor modules that correlated with immunophenotypes, the WGCNA was performed on the transcription factor profile of the ovarian cancer training cohort. After setting the soft threshold beta as 5 and cut height as 0.25, 10 transcription factor modules with different colors were identified (Fig. S2 and Fig. 1C). According to the correlations between modules and immunophenotypes, the turquoise, yellow and blue modules demonstrated stronger correlations with immunophenotypes than the remaining modules (Fig. 1D). Module significance analysis further demonstrated that the correlation coefficients between gene significance and module membership in turquoise, yellow and blue models reached 0.57, 0.89 and 0.40, respectively (Fig. 1E–G). So, these three modules were considered to be prominently associated with immunophenotypes and were selected for further analysis. A

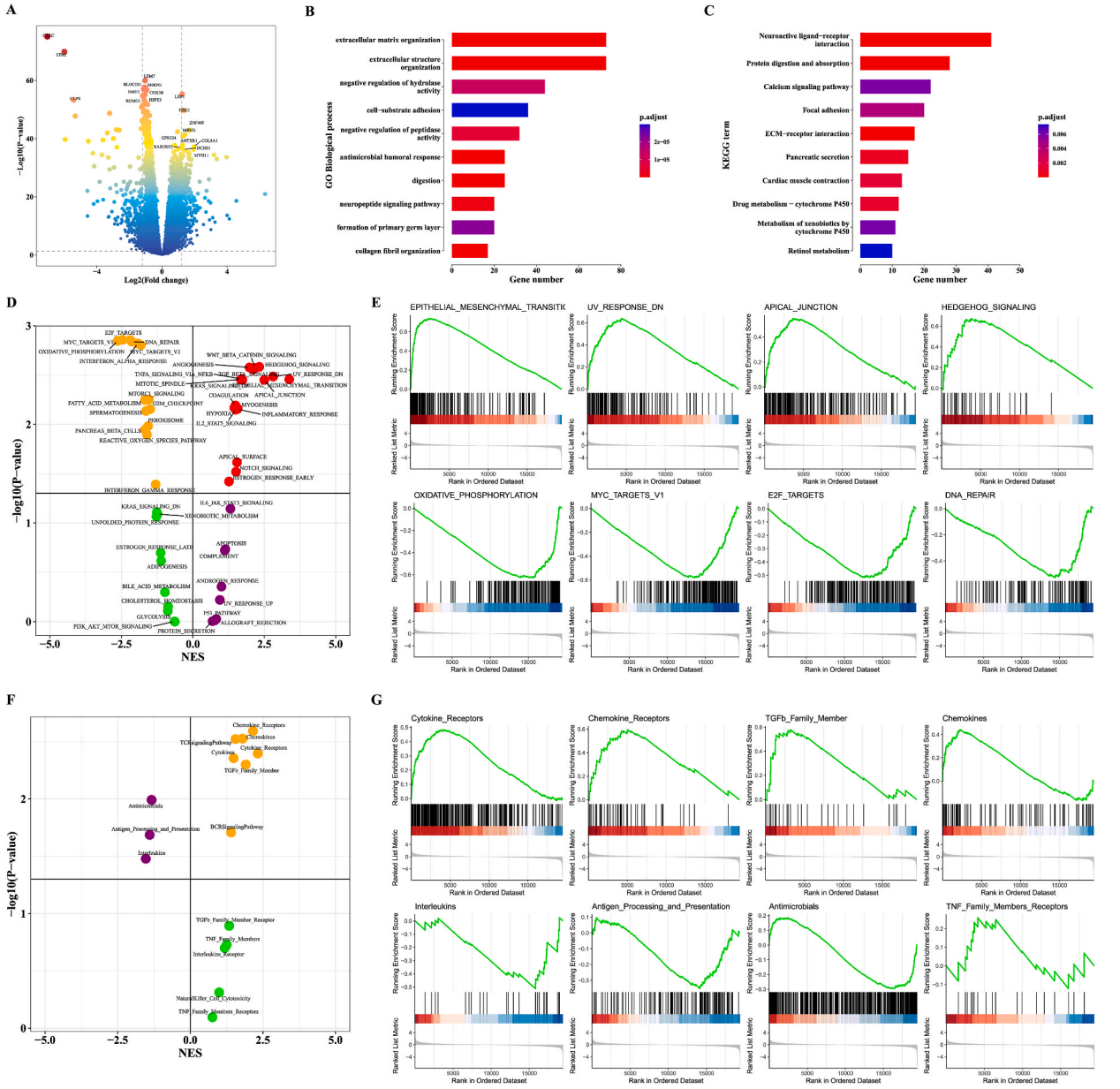

Fig. 4. Differentially expressed gene analyses of two different clustering subtypes in the TCGA cohort. (A) Volcano plot on differentially expressed genes between two ovarian cancer clustering subtypes. Enrichment analysis results for differentially expressed genes in **(B)** GO biological processes and **(C)** KEGG pathways. **(D)** Volcano plot illustrated the GSEA enrichment result for 50 Hallmark signatures. **(E)** GSEA enrichment results of 8 Hallmark signatures. **(F)** Volcano plot illustrated the GSEA enrichment result for 17 ImmPort immune signatures. **(G)** GSEA enrichment results of 8 ImmPort immune signatures.

total of 868 transcription factors in these three modules were regarded as immune-related transcription factors.

3.2. Construction of two transcription factor activity subtypes

In the training cohort, 67 prognostic transcription factors (*P*-value<0.001 and Hazard ratio>1; Log-rank test) were identified by the univariate Cox analysis from the protein activity profiles of 868 immune-related transcription factors (Supplementary Table 1). Then, the random survival tree analysis [51–53] was performed on these 67 transcription factors to rank the variables by importance, utilizing 1000 trees. ZNF384 was ranked as the most important variable and 15 important variables were selected (Fig. 2A and B). Based on the protein activity profiles of 15 transcription factors, the K-means clustering method was utilized to identify heterogeneous subtypes of ovarian cancer. The average silhouette width was explored to determine stable and robust subtypes of ovarian cancer patients, and the results revealed that the optimal clustering number was obtained when k = 2 (Fig. 2C). Two robust subtypes of transcription factors, referred to as cluster 1 and cluster 2, were identified in the training cohort.

To demonstrate the clinical relevance of the identified subtypes, a Kaplan-Meier analysis was conducted on the training cohort. As shown in Fig. 2D, patients in cluster 1 had significantly worse overall survival than those in cluster 2 (*P*-value = 1.21E-9; Log-rank test). Subsequently, the differences in the activity of 15 transcription factors between two ovarian cancer subtypes were investigated. Patients in cluster 1 exhibited significantly higher levels of transcription factor activity compared to those in cluster 2 (Fig. 2E; *P*-value<0.001; Wilcoxon rank-sum test).

Next, we evaluated the prognosis value of subtypes in the TCGA cohort of 421 ovarian cancer patients by conducting the Kaplan-Meier analysis. Consistently, the results illustrated that patients with cluster 1 exhibited worse overall survival, and a Log-rank *P*-value of 1.56E-2 was achieved between the two subtypes (Fig. 3A). Additionally, significant differences were found between two TCGA subtypes according to the Wilcoxon rank-sum test (Fig. 3B). The deep learning network [17,18,30,32,33,54] was used to predict ovarian cancer clustering subtypes based on transcription factor activity profile. The best hyper-parameters of the deep neural network were optimized by the grid search algorithm, and this model was further evaluated via the ten-fold cross-validation [54,55]. The predictive results indicated that the overall accuracy was 93.39% and the area under the ROC curve was 0.9929 in the training cohort (Fig. S3), demonstrated the robustness of the model in predicting the subtypes of ovarian cancer. To further verify the performance of the deep learning model, the subtypes of the ovarian cancer testing cohort were further predicted. The prognosis value of predicted subtypes exhibited that cluster 2 displayed an inferior prognosis at the overall survival level (Fig. 3C; *P*-value = 1.48E-3; Log-rank test). According to the Wilcoxon rank-sum test, the difference between two testing subtypes in 15 transcription factors was significant (Fig. 3D).

3.3. Differential genes enriched for two clustering subtypes in the TCGA cohort

Differential gene analysis was conducted between cluster 1 and cluster 2 subtypes, which identified 453 up-regulated and 483 down-regulated genes in the TCGA cohort (Fig. 4A; *P*-value<0.05 and $|\log_2 FC|<1$). In order to gain a comprehensive understanding of the underlying biological mechanisms affected by our subtypes, a systematic biological analysis was conducted to evaluate the function of differentially expressed genes (DEGs) between the two clustering subtypes in the TCGA cohort. The results of the GO biological processes enrichment analysis indicated that the DEGs were predominantly enriched in the extracellular matrix organization, cell-substrate adhesion, and negative regulation of peptidase activity (Fig. 4B). The results of the KEGG pathway enrichment analysis indicated that the DEGs were predominantly enriched in several pathways, including neuroactive ligand-receptor interaction, protein digestion and absorption, calcium signaling pathway and focal adhesion (Fig. 4C). The GSEA was performed to further investigate which Hallmark signatures and ImmPort immune signatures were correlated with the clustering subtypes in the TCGA cohort.

Analysis of the 50 gene sets of Hallmark signatures revealed that 18 signatures were positively correlated and 14 signatures were negatively correlated with the clustering subtype. (Fig. 4D). Among the signatures analyzed, the one exhibiting the highest NES value was EPITHELIAL MESENCHYMAL TRANSITION (EMT), which was a collection of genes associated with organ fibrosis and the initiation of metastasis in cancer progression (Fig. 4E). Additionally, the results from the ImmPort immune signature GSEA revealed that seven signatures were positively correlated, whereas three signatures were negatively correlated with the clustering subtype (Fig. 4F and G).

3.4. Construction of the ceRNA network in the TCGA cohort

In this study, the lncRNA and miRNA differential expression analysis was also performed between two clustering subtypes. Using the regulatory relationships between miRNA-mRNA and miRNA-lncRNA, a ceRNA network of lncRNA-miRNA-mRNA was constructed. This ceRNA network enabled the identification of significant regulatory pairs between two clustering subtypes. A total of 465 differentially expressed lncRNAs (dif-lncRNAs) were identified between two clustering subtypes in the TCGA cohort, of which 401 were up-regulated and 64 were down-regulated lncRNAs ($|\log_2 FC|>1.0$ and *P*-value<0.05). In the TCGA cohort, 82 up-regulated miRNAs and 54 down-regulated miRNAs were identified ($|\log_2 FC|>1.0$ and *P*-value<0.05). A total of 972 up-regulated mRNAs and 531 down-regulated mRNAs were also identified ($|\log_2 FC|>1.0$ and *P*-value<0.05). The 465 dif-lncRNAs were analyzed using the Bioconductor package multiMiR (version 1.18.0) [56] to identify potential miRNAs targeting lncRNAs. Three validated miRNA-mRNA databases [57], (miRecords [58], miRTarbase [59], and Tarbase [60]), were utilized to identify the downstream target mRNAs in reference to differentially expressed miRNAs (dif-miRNAs). Finally, a total of 9 lncRNAs (7 up-regulated and 2 down-regulated), 21

miRNAs (10 up-regulated and 11 down-regulated), and 231 up-regulated mRNAs were included to construct the lncRNA-miRNA-mRNA triple regulatory network (Fig. 5A). The detailed information of the ceRNA network was displayed in Supplementary Table 2 and Supplementary Table 3.

To further explore the potential functions associated with the lncRNA-miRNA-mRNA triple regulatory network, the functional enrichment analysis of GO biological processes and KEGG pathways was performed by the Bioconductor package clusterProfile. Among the 231 dif-mRNAs that were up-regulated, the GO biological process enrichment analysis revealed significant enrichment in processes related to translational initiation, protein targeting to membrane, viral gene expression, and other functions (Fig. 5B). The KEGG pathway enrichment analysis revealed a significant enrichment of up-regulated dif-mRNAs in various KEGG pathways, including the Ribosome pathway, Coronavirus disease-COVID-19 pathway, and Huntington disease pathway, among others (Fig. 5C).

3.5. Differential gene co-expression network analysis in the TCGA cohort

In this study, the Multi-scale Embedded Gene Co-expression Network Analysis (MEGENA) [61] was utilized to identify the differential gene co-expression networks between two clustering subtypes in the TCGA cohort. Compared with patients in cluster 1, 79, 604 differential gene network modules that enriched in cluster 2 were identified by the MEGENA algorithm [62]. Since the enriched modules in cluster 1 were identified in the TCGA cohort, the WGCNA was applied to further examine their correlation with the clustering subtype. A total of 38 enriched gene co-expression network modules, which showed an absolute correlation >0.5 with the clustering subtype, were identified (Fig. 6A). The 38 enriched gene co-expression network modules that were associated with cluster 1 were further examined using network analysis to identify hub genes and their associated degree values. Of the identified hub genes, GRHL2 exhibited the highest degree, with 245 interactions with other nodes in the network module (Fig. 6B). Meanwhile, KEGG enrichment analysis was also conducted on these modular genes (Supplementary Table 4). Among them, the c1 180 gene module showed the strongest correlation with the clustering subtypes (correlation coefficient = 0.64). 12 genes in the c1 180 gene module were found to be significantly enriched in multiple KEGG cancer pathways, such as the VEGF signaling pathway, T cell receptor signaling pathway, and ErbB signaling pathway.

Next, the normalized ssGSEA scores were calculated for 38 enriched gene co-expression network modules, using all genes within

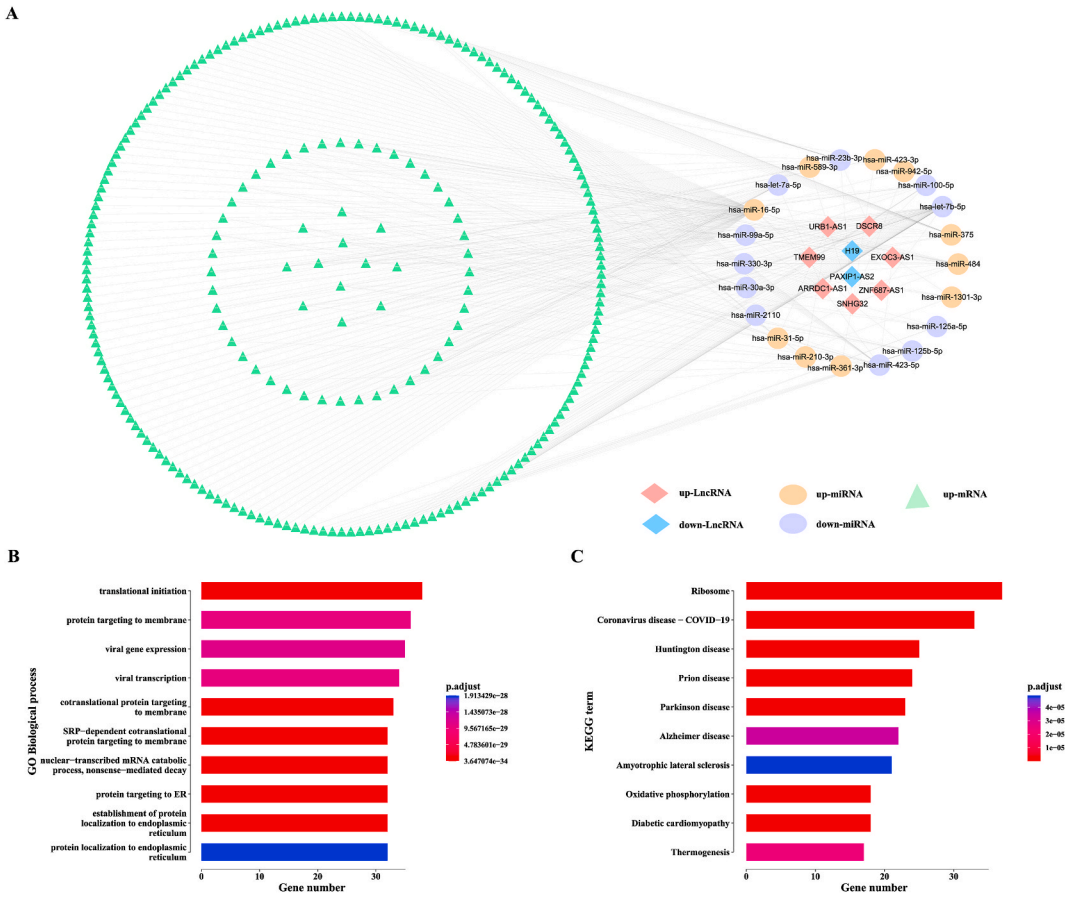

Fig. 5. The ceRNA network in the TCGA cohort. (A) The lncRNA-miRNA-mRNA network for the TCGA cohort. The top 10 enriched **(B)** GO biological processes and **(C)** KEGG pathways for the differentially expressed mRNAs in the ceRNA network.

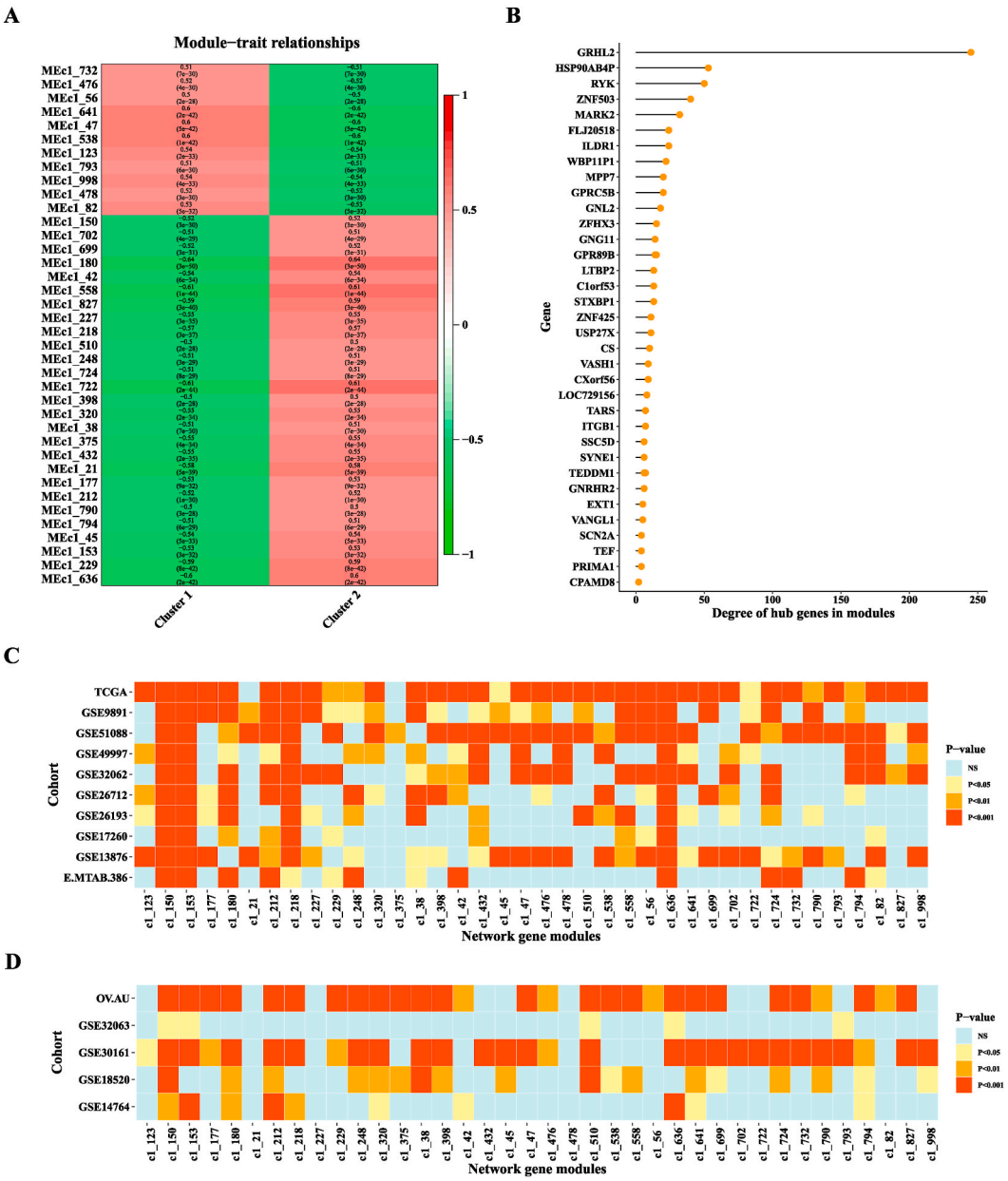

Fig. 6. Differential gene co-expression network analyses in the TCGA cohort. (A) The correlation between 38 enriched gene co-expression network modules and two clustering subtypes. **(B)** The degree values of hub genes for differential gene co-expression network modules between two clustering subtypes. Tile plot of 38 significantly enriched gene co-expression network modules for each ovarian cancer dataset in **(C)** the training cohort and **(D)** the testing cohort. The color in the tile plot corresponded to the *P*-values that calculated from the different ssGSEA scores between two clustering subtypes (Wilcoxon rank-sum test).

each respective network module as the gene set. Upon comparing the ssGSEA scores for 38 enriched gene co-expression network modules in cluster 1 versus cluster 2 in the training cohort, we observed that most gene modules showed significantly higher enrichment in cluster 1 across various datasets within the training cohort. Specifically, approximately 95% (36 out of 38) of the gene modules in the TCGA cohort displayed significantly higher enrichment in cluster 1 with a P-value<0.05, as determined by the Wilcoxon rank-sum test. (Fig. 6C). Furthermore, these gene network modules were assessed in the testing cohorts. Similar results were also observed in the OVAU and GSE30161 cohorts (Fig. 6D).

3.6. Associations of clustering subtypes for predicting chemotherapy and immunotherapy response in the TCGA cohort

In this section, a study was conducted to investigate the impact of clustering subtypes on chemotherapy response within the TCGA

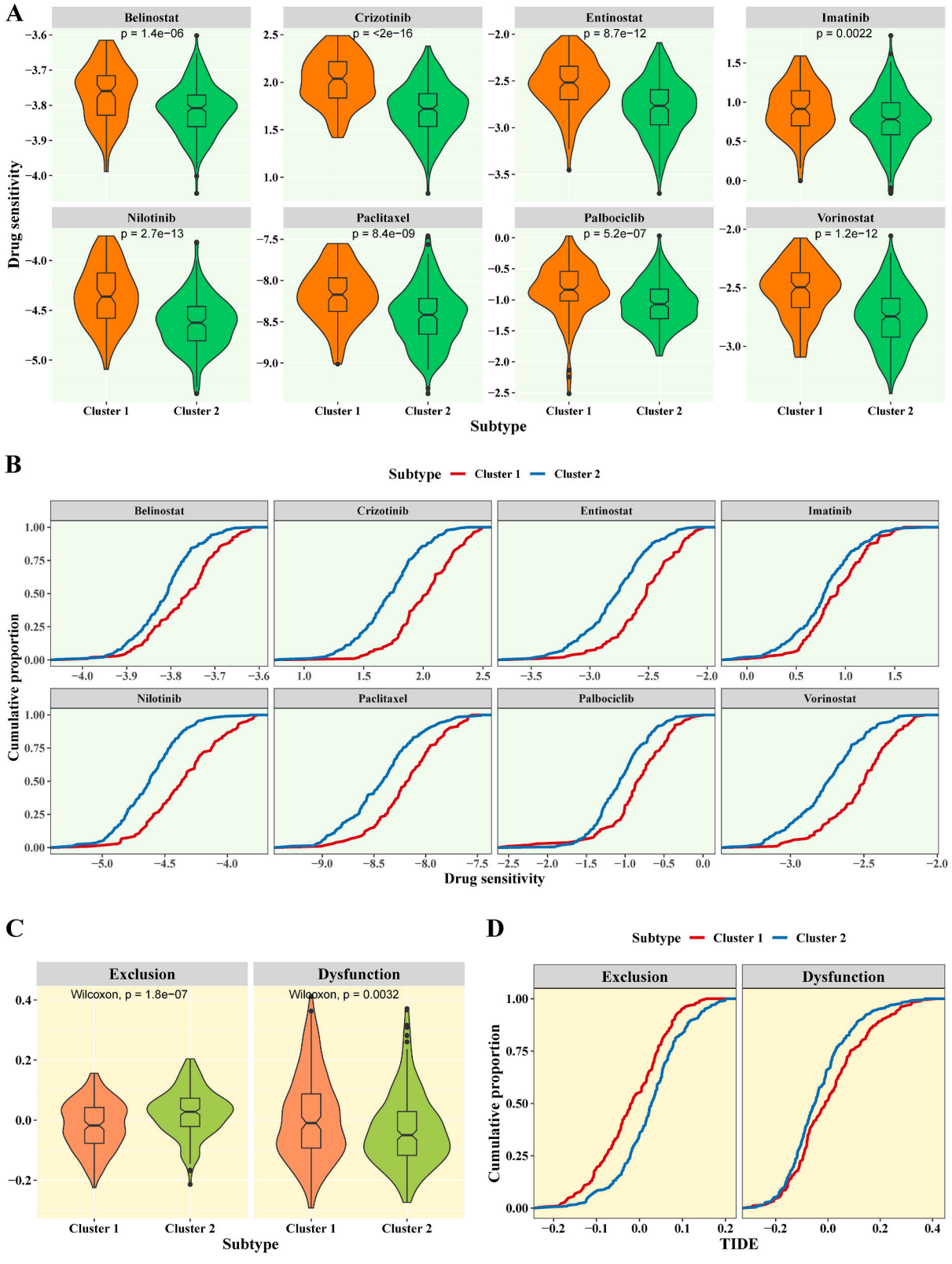

(caption on next page)

Fig. 7. Comparison of chemotherapy and immunotherapy response between two different clustering subtypes in the TCGA cohort. **(A)** Violin plots illustrated the IC_{50} values of 8 anticancer drugs between two different clustering subtypes. **(B)** Cumulative probability of IC_{50} values of 8 anticancer drugs in two different clustering subtypes. **(C)** Violin plots illustrated the exclusion and dysfunction between two different clustering subtypes. **(D)** Cumulative probability of the exclusion and dysfunction in two different clustering subtypes.

cohort. The chemotherapeutic drug sensitivity analysis was focused on 8 commonly used anticancer drugs in the GDSC database for the TCGA ovarian cancer samples. Upon conducting the Wilcoxon rank-sum test, we discovered 8 anticancer drugs exhibited greater sensitivity in cluster 2, with significantly lower IC_{50} values for patients in cluster 2 (Fig. 7A). Furthermore, the cumulative frequency distribution of IC_{50} values for patients in cluster 2 was distinguishable from that of patients in cluster 1. This observation provided further validation for the drug sensitivity results presented earlier (Fig. 7B).

The sensitivity of 251 chemotherapeutic drugs in the GDSC database for TGCA patients was analyzed. To determine differences between the two subtypes, a Wilcoxon rank-sum test was conducted on the IC_{50} values of 251 GDSC chemotherapeutic drugs. According to the Wilcoxon rank-sum test, the IC_{50} values of 163 GDSC chemotherapeutic drugs between two clustering subtypes were significantly different. Specifically, 111 (68.1%) of the drugs were found to be more resistant in cluster 2 samples, while 52 (31.9%) were more sensitive (Supplementary Table 5). Given the current context, it is possible that GDSC chemotherapeutic drugs could demonstrate efficacy in the treatment of ovarian cancer patients classified under cluster 2 in the future. Next, we evaluated the response of the two clustering subtypes to immune checkpoint blockade treatment by measuring their T cell dysfunction and exclusion scores. The cluster 1 subtype exhibited higher T cell dysfunction scores and lower exclusion scores than the cluster 2 subtype, as illustrated in Fig. 7C. In contrast, the cumulative distribution of T cell dysfunction and exclusion scores presented opposite findings, as illustrated in Fig. 7D. These findings suggested that the cluster 1 subtype may have higher levels of T cell infiltration, indicating that immunotherapy could be more effective in restoring dysfunctional T cells in this subtype.

4. Discussion

After receiving external stimuli, cells activate certain transcription factors, which bind to specific sites on DNA molecules and attract RNA polymerase to the transcription factor initiation sites of the associated genes, thus initiating transcription [63]. Transcription factors play important roles in living organisms by regulating multiple upstream and downstream genes and thus have become a hotspot in studies of functionally important genes. In living organisms, transcription factor activity is among the critical determinants of the regulation degree of associated target genes [64,65]. In recent years, transcription factor activity has been predicted based on gene expression profiles of regulons to characterize the functional status of transcriptional regulatory circuits [64, 66–68]. Moreover, transcription factor activity has been widely examined in cancer-related studies. In this study, we inferred the protein activity of transcription factors by examining the mRNA levels of their direct transcriptional targets rather than focusing solely on the gene expression of the transcription factors themselves. This approach provided a more accurate reflection of gene interactions and was more consistent with the intricate and multifaceted nature of gene regulation within the human body. Compared with gene expression data, transcription factor activity can extract more functional insight from transcriptomic data, and reveal known and novel mechanisms involved in tumor development. In addition, transcription factor activity provides a more nuanced and dynamic view of gene regulation compared to gene expression analysis alone. By using this method, we were able to better understand the actual function of transcription factors in the context of human biology.

Among 8 anticancer drugs, paclitaxel is a frequently utilized drug for the treatment of ovarian cancer [69]. In clinical trials, belinostat and crizotinib have demonstrated clinical benefits when combined with other drugs for the treatment of ovarian cancer [70, 71]. Entinostat enhances olaparib-induced DNA damage, thereby strengthening antitumor efficacy [72]. Imatinib has been shown to impede ovarian cancer cell growth by arresting cells in the G0-G1 phase and preventing their progression to the S phase [73]. Nilotinib has been found to effectively reduce the activity of ovarian cancer cells through mitochondria-dependent apoptosis [74]. Palbociclib induces reactive cell cycle arrest and senescence, leading to antitumor effects [75]. Lastly, vorinostat inhibits the polarization of M2 macrophages and reduces the size of ovarian tumors [76]. These findings highlight the potential of various drugs in the treatment of ovarian cancer.

In this study, we used the Human DoRothEA dataset compiled by Garcia-Alonso et al. [37], which described 454,504 interactions between 1332 human transcription factors and 20,295 associated target genes. The Human DoRothEA dataset is a comprehensive resource of human transcriptional regulatory network, which has been used in numerous studies to investigate the transcription factors and their associated target genes. Based on the gene expression profile data in the training cohorts and data in the Human DoRothEA dataset, we calculated the activity of 1332 transcription factors. Based on the WGCNA method, we identified 868 transcription factors associated with immunity and got 15 transcription factors associated with prognosis by further analysis. Among these 15 transcription factors, HOXC4 is a member of the homeobox family of transcription factors that promotes ovarian cancer cell proliferation, migration, invasion, and tumor formation through the regulation of various genes and pathways [77]. ZNF699 has been shown to promote tumor cell proliferation and invasion by regulating genes involved in the cell cycle and apoptosis. IRX6 has been shown to regulate genes that involve in the cell cycle and this transcription factor has been associated with poor ovarian cancer patient prognosis. Through a univariate Cox analysis, we found that the protein activity of all these 15 transcription factors was significantly associated with poor prognosis in the ovarian cancer patients. With the activity profile of these 15 transcription factors, the ovarian cancer patients were classified into different genomic subtypes, which illustrated significant differences in overall survival time. Meanwhile, the molecular subtypes identified in this study accurately reflected the differentiated sensitivity of chemotherapeutic drugs in the GDSC, suggesting

that such molecular subtypes can be used as biomarkers for evaluating the efficacy of ovarian cancer chemotherapy. Moreover, the transcriptional activity subtypes showed differences in immune signature scores, indicated that different subtypes varied in the level of T cell infiltration, and the cluster 1 subtype tended to be more sensitive to immunotherapy.

MEGENA is a graph embedding-based tool for constructing gene co-expression networks that can be used to perform similarity analysis based on gene expression profiles and thus construct a planar-filtered network. Multiscale clustering analysis can be performed on the modules in a planar-filtered network. MEGENA is a robust tool for analyzing gene expression data across various tissues or cell types. It can effectively identify critical gene models involved in specific biological processes or diseases, providing a comprehensive understanding of biological mechanisms and disease etiologies. In this study, to refine differences between two transcription factor activity clustering subtypes at the gene expression level, we identified 38 gene co-expression network modules of two subtypes in the TCGA cohort with MEGENA. These modules differed significantly not only between two clustering subtypes in the TCGA cohort, but also between the GSE9891, GSE51088, GSE49997, GSE32062, GSE13876, OVAU, and GSE30161 cohorts. In addition, in the c1 180 gene module, the PIK3CB gene encodes the catalytic subunit of the phosphoinositide 3-kinase (PI3K) gene family; PI3K signaling pathways are among those most prone to change in human cancers, and dysregulation of these pathways typically leads to tumorigenesis and progression. These results demonstrated that the gene modules we identified differed extensively across multiple datasets and these modular genes could account for a degree of heterogeneity in two transcriptional activity subtypes.

The study has some limitations that should be acknowledged. First, we exclusively utilized public ovarian cancer cohorts due to the unavailability of sequencing ovarian cancer samples. Second, in the present investigation, drug sensitivities for distinct clustering subtypes were evaluated. Notably, the determination of drug IC_{50} values was not based on conventional experimentation, but rather on computational algorithms. So, more in vivo or in vitro experiments should be conducted to further validate the drug sensitivities of these drugs.

In conclusion, the clustering subtypes associated with the prognosis of ovarian cancer patients can be identified based on the activity data of transcription factor proteins. Many genomic studies have been performed to evaluate the molecular subtypes of patients with cancer. Based on the good performance of the transcription factor clustering model in predicting the prognosis and chemotherapy effects of patients with ovarian cancer, further studies should be performed to increase the data and confirm the transcription factor activity profiles of patients with cancer. Our results show clinical potential for ovarian cancer subtyping and can assist in determining personalized therapies.

Author contribution statement

Yongchun Zuo and Lei Yang: conceived and designed the experiments. Yuqiang Xiong, Haodong Wei and Jiawei Ke: performed the experiments. Haoxin Zhang and Yao Yu: analyzed and interpreted the data. Pengfei Liang and Shiyuan Wang: contributed reagents, materials, analysis tools or data, and wrote the paper.

Funding statement

This work was supported by the National Natural Science Foundation of China (No.32000473 and No. 62173117), Natural Science Foundation of Heilongjiang Province (LH2020C100), the Heilongjiang Postdoctoral Research Startup Foundation (LBH-Q19118) and the Cooperative Scientific Research Project of “Chunhui plan” for Ministry of Education (HLJ201919).

Data availability statement

All sequencing data applied in this study is freely accessible at the corresponding database described above. The source codes of this study were available from GitHub at: https://github.com/LeiyangHarbin/Heliyon.

Declaration of competing interest

The authors declare that they have no known competing financial interests or personal relationships that could have appeared to influence the work reported in this paper.

Appendix A. Supplementary data

Supplementary data to this article can be found online at https://doi.org/10.1016/j.heliyon.2023.e16147.

References

[1] R.L. Siegel, K.D. Miller, H.E. Fuchs, et al., Cancer statistics, CA A Cancer J. Clin. 71 (2021) 7–33.
[2] H. Sung, J. Ferlay, R.L. Siegel, et al., Global Cancer Statistics 2020: GLOBOCAN estimates of Incidence and mortality worldwide for 36 cancers in 185 countries, CA A Cancer J. Clin. 71 (2021) 209–249.
[3] R.L. Siegel, K.D. Miller, H.E. Fuchs, et al., Cancer statistics, CA A Cancer J. Clin. 72 (2022) 7–33.

[4] R.L. Siegel, K.D. Miller, N.S. Wagle, et al., Cancer statistics, CA A Cancer J. Clin. 73 (2023) 17–48.
[5] H. Li, X. Zheng, J. Gao, et al., Whole transcriptome analysis reveals non-coding RNA's competing endogenous gene pairs as novel form of motifs in serous ovarian cancer, Comput. Biol. Med. 148 (2022), 105881.
[6] H. Nada, K. Lee, L. Gotina, et al., Identification of novel discoidin domain receptor 1 (DDR1) inhibitors using E-pharmacophore modeling, structure-based virtual screening, molecular dynamics simulation and MM-GBSA approaches, Comput. Biol. Med. 142 (2022), 105217.
[7] H. Zhang, M. Chi, D. Su, et al., A random forest-based metabolic risk model to assess the prognosis and metabolism-related drug targets in ovarian cancer, Comput. Biol. Med. 153 (2023), 106432.
[8] J. Zhou, W. Cao, L. Wang, et al., Application of artificial intelligence in the diagnosis and prognostic prediction of ovarian cancer, Comput. Biol. Med. 146 (2022), 105608.
[9] A.-M. Patch, E.L. Christie, D. Etemadmoghadam, et al., Whole–genome characterization of chemoresistant ovarian cancer, Nature 521 (2015) 489–494.
[10] S. Kumar, P. Paul, P. Yadav, et al., A multi-targeted approach to identify potential flavonoids against three targets in the SARS-CoV-2 life cycle, Comput, Biol. Med. 142 (2022), 105231.
[11] G. Radha, P.K. Naik, M. Lopus, In vitro characterization and molecular dynamic simulation of shikonin as a tubulin-targeted anticancer agent, Comput. Biol. Med. 147 (2022), 105789.
[12] Z. Lv, F. Cui, Q. Zou, et al., Anticancer peptides prediction with deep representation learning features, Briefings Bioinf. 22 (2021) bbab008.
[13] S. Armbruster, R.L. Coleman, J.A. Rauh-Hain, Management and treatment of recurrent epithelial ovarian cancer, Hematol. Oncol. Clin. N. Am. 32 (2018) 965–982.
[14] S.A. Lambert, A. Jolma, L.F. Campitelli, et al., The human transcription factors, Cell 172 (2018) 650–665.
[15] D.Y. Liu, G.P. Li, Y.C. Zuo, Function determinants of TET proteins: the arrangements of sequence motifs with specific codes, Briefings Bioinf. (2019) 1826–1835.
[16] B. Xu, D. Liu, Z. Wang, et al., Multi-substrate selectivity based on key loops and non-homologous domains: new insight into ALKBH family, Cell. Mol. Life Sci. 78 (2021) 129–141.
[17] P. Zhang, Y. Wu, H. Zhou, et al., CLNN-loop: a deep learning model to predict CTCF-mediated chromatin loops in the different cell lines and CTCF-binding sites (CBS) pair types, Bioinformatics 38 (2022) 4497–4504.
[18] P. Zhang, H. Zhang, H. Wu, iPro-WAEL: a comprehensive and robust framework for identifying promoters in multiple species, Nucleic Acids Res. 50 (2022) 10278–10289.
[19] Q. Zhang, H. Li, Y. Liu, et al., Exosomal non-coding RNAs: new insights into the biology of hepatocellular carcinoma, Curr. Oncol. (2022) 5383–5406.
[20] L. Zheng, D. Liu, Y.A. Li, et al., RaacFold: a webserver for 3D visualization and analysis of protein structure by using reduced amino acid alphabets, Nucleic Acids Res. 50 (2022) W633–W638.
[21] J.M. Vaquerizas, S.K. Kummerfeld, S.A. Teichmann, et al., A census of human transcription factors: function, expression and evolution, Nat. Rev. Genet. 10 (2009) 252–263.
[22] M. Yu, J. Zhan, H. Zhang, HOX family transcription factors: related signaling pathways and post-translational modifications in cancer, Cell. Signal. 66 (2020), 109469.
[23] M. Duan, Y. Wang, Y. Qiao, et al., Pan-cancer identification of the relationship of metabolism-related differentially expressed transcription regulation with non-differentially expressed target genes via a gated recurrent unit network, Comput. Biol. Med. 148 (2022), 105883.
[24] M. Duan, L. Zhang, Y. Wang, et al., Computational pan-cancer characterization of model-based quantitative transcription regulations dysregulated in regional lymph node metastasis, Comput. Biol. Med. 135 (2021), 104571.
[25] T.B. Nguyen, D.N. Do, M.-L. Nguyen-Thi, et al., Identification of potential crucial genes and key pathways shared in Inflammatory Bowel Disease and cervical cancer by machine learning and integrated bioinformatics, Comput. Biol. Med. 149 (2022), 105996.
[26] Z. Lv, J. Zhang, H. Ding, et al., RF-PseU: a random forest predictor for RNA pseudouridine sites, Front. Bioeng. Biotechnol. 8 (2020).
[27] H. Li, C. Long, J. Xiang, et al., Dppa2/4 as a trigger of signaling pathways to promote zygote genome activation by binding to CG-rich region, Briefings Bioinf. 22 (2021) bbaa342.
[28] C.Z. Ma, M.R. Brent, Inferring TF activities and activity regulators from gene expression data with constraints from TF perturbation data, Bioinformatics 37 (2021) 1234–1245.
[29] T. Schacht, M. Oswald, R. Eils, et al., Estimating the activity of transcription factors by the effect on their target genes, Bioinformatics 30 (2014) i401–i407.
[30] J. Jiang, X. Lin, Y. Jiang, et al., Identify bitter peptides by using deep representation learning features, Int. J. Mol. Sci. (2022) 7877.
[31] L. Zhang, Y. Yang, L. Chai, et al., A deep learning model to identify gene expression level using cobinding transcription factor signals, Briefings Bioinf. 23 (2022) bbab501.
[32] Z. Zhang, H. Chai, Y. Wang, et al., Cancer survival prognosis with deep bayesian perturbation Cox network, Comput. Biol. Med. 141 (2022), 105012.
[33] T. Yu, N. Lin, X. Zhong, et al., Multi-label recognition of cancer-related lesions with clinical priors on white-light endoscopy, Comput. Biol. Med. 143 (2022), 105255.
[34] L. Yang, S.Y. Wang, Q. Zhang, et al., Clinical significance of the immune microenvironment in ovarian cancer patients, Mol Omics 14 (2018) 341–351.
[35] S. Bentink, B. Haibe-Kains, T. Risch, et al., Angiogenic mRNA and microRNA gene expression signature predicts a novel subtype of serous ovarian cancer, PLoS One 7 (2012), e30269.
[36] E. Cerami, J. Gao, U. Dogrusoz, et al., The cBio Cancer Genomics Portal: an open platform for exploring multidimensional cancer genomics data, Cancer Discov. 2 (2012) 401–404.
[37] L. Garcia-Alonso, C.H. Holland, M.M. Ibrahim, et al., Benchmark and integration of resources for the estimation of human transcription factor activities, Genome Res. 29 (2019) 1363–1375.
[38] M.J. Alvarez, Y. Shen, F.M. Giorgi, et al., Functional characterization of somatic mutations in cancer using network-based inference of protein activity, Nat. Genet. 48 (2016) 838–847.
[39] M.D. Robinson, D.J. McCarthy, G.K. Smyth, edgeR: a Bioconductor package for differential expression analysis of digital gene expression data, Bioinformatics 26 (2010) 139–140.
[40] M.-L. Shih, J.-C. Lee, S.-Y. Cheng, et al., Transcriptomic discovery of a theranostic signature (SERPINE1/MMP3/COL1A1/SPP1) for head and neck squamous cell carcinomas and identification of antrocinol as a candidate drug, Comput, Biol. Med. 150 (2022), 106185.
[41] A. Ozhan, M. Tombaz, O. Konu, SmulTCan: a Shiny application for multivariable survival analysis of TCGA data with gene sets, Comput. Biol. Med. 137 (2021), 104793.
[42] T. Wu, E. Hu, S. Xu, et al., clusterProfiler 4.0: a universal enrichment tool for interpreting omics data, Innovation (2021), 100141.
[43] S. Hänzelmann, R. Castelo, J. Guinney, GSVA: gene set variation analysis for microarray and RNA-seq data, BMC Bioinf. 14 (2013) 7.
[44] A. Subramanian, P. Tamayo, V.K. Mootha, et al., Gene set enrichment analysis: a knowledge-based approach for interpreting genome-wide expression profiles, Proc. Natl. Acad. Sci. U. S. A 102 (2005) 15545–15550.
[45] A. Liberzon, C. Birger, H. Thorvaldsdóttir, et al., The molecular signatures database hallmark gene set collection, Cell Syst 1 (2015) 417–425.
[46] S. Bhattacharya, P. Dunn, C.G. Thomas, et al., ImmPort, toward repurposing of open access immunological assay data for translational and clinical research, Sci. Data 5 (2018), 180015.
[47] P. Langfelder, S. Horvath, WGCNA: an R package for weighted correlation network analysis, BMC Bioinf. 9 (2008) 559.
[48] W. Yang, J. Soares, P. Greninger, et al., Genomics of Drug Sensitivity in Cancer (GDSC): a resource for therapeutic biomarker discovery in cancer cells, Nucleic Acids Res. 41 (2013) D955–D961.
[49] P. Jia, R. Hu, G. Pei, et al., Deep generative neural network for accurate drug response imputation, Nat. Commun. 12 (2021) 1740.
[50] P. Jiang, S. Gu, D. Pan, et al., Signatures of T cell dysfunction and exclusion predict cancer immunotherapy response, Nat. Med. 24 (2018) 1550–1558.
[51] H. Ishwaran, U.B. Kogalur, E.H. Blackstone, et al., Random survival forests, Ann. Appl. Stat. 2 (2008) 841–860.
[52] L. Breiman, Random forests, Mach. Learn. 45 (2001) 5–32.

[53] K.L. Pickett, K. Suresh, K.R. Campbell, et al., Random survival forests for dynamic predictions of a time-to-event outcome using a longitudinal biomarker, BMC Med. Res. Methodol. 21 (2021) 216.
[54] Y. Yang, D. Gao, X. Xie, et al., DeepIDC: a prediction framework of injectable drug combination based on heterogeneous information and deep learning, Clin. Pharmacokinet. 61 (2022) 1749–1759.
[55] Z. Sun, Q. Huang, Y. Yang, et al., PSnoD: identifying potential snoRNA-disease associations based on bounded nuclear norm regularization, Briefings Bioinf. 23 (2022) bbac240.
[56] Y. Ru, K.J. Kechris, B. Tabakoff, et al., The multiMiR R package and database: integration of microRNA–target interactions along with their disease and drug associations, Nucleic Acids Res. 42 (2014) e133.
[57] A. Kozomara, M. Birgaoanu, S. Griffiths-Jones, miRBase: from microRNA sequences to function, Nucleic Acids Res. 47 (2019) D155–D162.
[58] F. Xiao, Z. Zuo, G. Cai, et al., miRecords: an integrated resource for microRNA–target interactions, Nucleic Acids Res. 37 (2009) D105–D110.
[59] H.-Y. Huang, Y.-C.-D. Lin, J. Li, et al., miRTarBase 2020: updates to the experimentally validated microRNA–target interaction database, Nucleic Acids Res. 48 (2020) D148–D154.
[60] D. Karagkouni, M.D. Paraskevopoulou, S. Chatzopoulos, et al., DIANA-TarBase v8: a decade-long collection of experimentally supported miRNA–gene interactions, Nucleic Acids Res. 46 (2018) D239–D245.
[61] W.-M. Song, B. Zhang, Multiscale embedded gene Co-expression network analysis, PLoS Comput. Biol. 11 (2015), e1004574.
[62] A.T. McKenzie, I. Katsyv, W.-M. Song, et al., DGCA: A comprehensive R package for differential gene correlation analysis, BMC Syst. Biol. 10 (2016) 106.
[63] Z. Wang, D. Liu, B. Xu, et al., Modular arrangements of sequence motifs determine the functional diversity of KDM proteins, Briefings Bioinf. 22 (2021) bbaa215.
[64] L. Garcia-Alonso, F. Iorio, A. Matchan, et al., Transcription factor activities enhance markers of drug sensitivity in cancer, Cancer Res. 78 (2018) 769–780.
[65] H.S. Li, N. Ta, C.S. Long, et al., The spatial binding model of the pioneer factor Oct4 with its target genes during cell reprogramming, Comput. Struct. Biotechnol. J. 17 (2019) 1226–1233.
[66] R. Mall, M. Saad, J. Roelands, et al., Network-based identification of key master regulators associated with an immune-silent cancer phenotype, Brief, Bioinformatics 22 (2021) bbab168.
[67] E.O. Paull, A. Aytes, S.J. Jones, et al., A modular master regulator landscape controls cancer transcriptional identity, Cell 184 (2021) 334–351.e320.
[68] K. Arumugam, W. Shin, V. Schiavone, et al., The master regulator protein BAZ2B can reprogram human hematopoietic lineage-committed progenitors into a multipotent state, Cell Rep. 33 (2020), 108474.
[69] E.K. Rowinsky, M.R. Gilbert, W.P. McGuire, et al., Sequences of taxol and cisplatin: a phase I and pharmacologic study, J. Clin. Oncol. 9 (1991) 1692–1703.
[70] D.S. Dizon, L. Damstrup, N.J. Finkler, et al., Phase II activity of belinostat (PXD-101), carboplatin, and paclitaxel in women with previously treated ovarian cancer, Int. J. Gynecol. Cancer 22 (2012) 979.
[71] D. Dong, G. Shen, Y. Da, et al., Successful treatment of patients with refractory high-grade serous ovarian cancer with GOPC-ROS1 fusion using crizotinib: a case report, Oncol. 25 (2020) e1720–e1724.
[72] V.G. Gupta, J. Hirst, S. Petersen, et al., Entinostat, a selective HDAC1/2 inhibitor, potentiates the effects of olaparib in homologous recombination proficient ovarian cancer, Gynecol. Oncol. 162 (2021) 163–172.
[73] D. Matei, D.D. Chang, M.-H. Jeng, Imatinib mesylate (gleevec) inhibits ovarian cancer cell growth through a mechanism dependent on platelet-derived growth factor receptor α and akt inactivation, Clin. Cancer Res. 10 (2004) 681–690.
[74] T.-C. Chen, M.-C. Yu, C.-C. Chien, et al., Nilotinib reduced the viability of human ovarian cancer cells via mitochondria-dependent apoptosis, independent of JNK activation, Toxicol. Vitro 31 (2016) 1–11.
[75] S. Llanos, D. Megias, C. Blanco-Aparicio, et al., Lysosomal trapping of palbociclib and its functional implications, Oncogene 38 (2019) 3886–3902.
[76] T.-H. Hsieh, C.-Y. Hsu, C.-W. Wu, et al., Vorinostat decrease M2 macrophage polarization through ARID1A6488delG/HDAC6/IL-10 signaling pathway in endometriosis-associated ovarian carcinoma, Biomed. Pharmacother. 161 (2023), 114500.
[77] N. Li, J-h Gou, J. Xiong, et al., HOXB4 promotes the malignant progression of ovarian cancer via DHDDS, BMC Cancer 20 (2020) 222.